Hybrid Energy Storage System Based on a Multioutput Multilevel Converter

Lizana, Ricardo; Rivera, Sebastian; Figueroa, Fidel; Flores-Bahamonde, Freddy; Rodriguez, Jose; Goetz, Stefan M.

DOI
10.1109/JESTPE.2023.3281760

Publication date
2023

Document Version
Final published version

Published in
IEEE Journal of Emerging and Selected Topics in Power Electronics

Hybrid Energy Storage System Based on a Multioutput Multilevel Converter

Ricardo Lizana, *Senior Member, IEEE*, Sebastian Rivera, *Senior Member, IEEE*, Fidel Figueroa, *Student Member, IEEE*, Freddy Flores-Bahamonde, *Senior Member, IEEE*, Jose Rodriguez, *Life Fellow, IEEE*, and Stefan M. Goetz, *Member, IEEE*

***Abstract*— Energy storage systems (ESSs) allow improving the stability and efficiency of the electrical grids with a high penetration of renewable energy sources. Moreover, the use of Hybrid ESSs (HESSs) enables storage solutions with both high-energy and high-power densities, by combining different storage technologies such as diverse battery chemistries, ultra-capacitors, or hydrogen fuel cells to name a few. In this article, an HESS-based multioutput multilevel (MOM) converter is presented. The proposed topology enables decoupled control of each ac converter voltage output. The internal switching states further allow the use of different storage units and high-quality multilevel voltage in each ac output. The mathematical model of the proposed topology and the defined operation region of the system, besides a model-predictive control strategy, are developed. Finally, simulation and experimental results validate the performance of the proposed topology.**

***Index Terms*— Energy storage system (ESS), modular multilevel series parallel converter (MMSPC), multioutput multilevel (MOM) converter.**

I. Introduction

ENERGY storage systems (ESSs) have become one of the key elements to develop smart and sustainable electrical grids. Their massive integration along with renewable energy systems (RESs) will boost existing electric facilities to ensure a reliable energy transition toward carbon-free energy system [1], [2], [3], [4], [5], [6]. Besides, they are also a crucial technology for higher electrification of the transportation sector, smoothing electric-vehicle (EV) charging demand, line congestion, or power quality issues, further expanding the capabilities of EV charging stations to stabilizing grid assets [6], [7], [8], [9]. In other words, ESSs are the key to support the energy transition of the electrical system at different levels.

In general, the operation of the electrical power grid is based on a rather precise matching between consumption and generation [8]. This conventional way leads to several operational drawbacks. For instance, delayed demand response due to the large grid inertia, instantaneous power mismatch between the generation and the consumption causing massive energy waste and reduced controllability [5], [6]. Indeed, it is expected that the instantaneous energy mismatch will be worsened with the increasing integration of RESs, given their inherent steep reduction in the system inertia.

Thus, ESSs connected in strategic sections of the grid could offer potential benefits encouraging the integration of RES, smoothing the demand response, providing ancillary services, and reducing the requirement of grid reinforcements [5], [9], [10], [11], [12]. To further improve their advantages, different storage technologies/mechanisms or a combination of them could be implemented depending on specific location requirements since they can provide different operational efficiencies, capacities, dynamic responses, and high-power densities [2], [5], [6]. In this sense, the use of hybrid storage systems will mix features like those composed of Lithium-ion batteries and ultra-capacitors (UCs), i.e., high capacity and fast response [13], [14].

For the optimal operation and control of Hybrid ESSs (HESSs), it is necessary to integrate power electronics converters that allow the internal balanced operation between the different storage units and loads. Moreover, power converters must provide modularity, scalability, and reliability, together with other direct benefits such as significant filter size reduction. To achieve these operating features, different multilevel converters have been presented in the literature as interesting solutions for HESS [15], [16], [17]. In [18], for instance, a modular multilevel series parallel converter (MMSPC) is proposed for a UC and batteries as storage units, offering dynamic reconfiguration for both series and parallel connections. Similarly, in [19] and [20] a Cascade Multilevel Converter (CMC)

Manuscript received 15 December 2022; revised 23 March 2023 and 7 May 2023; accepted 14 May 2023. Date of publication 31 May 2023; date of current version 2 August 2023. This work was supported in part by the Agencia Nacional de Investigación y Desarrollo (ANID): Fondo Nacional de Desarrollo Científico y Tecnológico (FONDECYT) under Grant 1230306, in part by REDES-Programa de Cooperación Internacional (PCI) under Grant 190108, in part by Advanced Center of Electrical and Electronic Engineering (AC3E) under Grant ANID/Basal/FB0008, in part by the Solar Energy Research Center (SERC) Chile under Grant ANID/FONDAP/1522A0006 and Grant ANID/EQM/180215, and in part by the Duke Energy Initiative and the Isaac Newton Trust of Trinity College Cambridge. Recommended for publication by Associate Editor Wuhua Li. *(Corresponding author: Ricardo Lizana.)*

Ricardo Lizana and Fidel Figueroa are with the Department of Electrical Engineering, Centro de Energía, Universidad Católica de la Santísima Concepción, Concepción 4090541, Chile (e-mail: ricardolizana@ucsc.cl).

Sebastian Rivera is with the Department of Electrical Sustainable Energy, DCE and S Group, Delft University of Technology, 2628 CD Delft, The Netherlands, and also with the Department of Electrical Engineering, Centro de Energía, Universidad Católica de la Santísima Concepción, Concepción 4090541, Chile (e-mail: s.rivera.i@ieee.org).

Freddy Flores-Bahamonde is with the Department of Engineering Sciences, Universidad Andres Bello, Santiago 7591538, Chile (e-mail: freddy.flores@unab.cl).

Jose Rodriguez is with the Faculty of Engineering, Universidad San Sebastian Santiago, Santiago 8370146, Chile (e-mail: jose.rodriguezp@uss.cl).

Stefan M. Goetz is with the Department of Engineering, University of Cambridge, CB3 0FA Cambridge, U.K., and also with the Department of Electrical Engineering, Duke University, Durham, NC 27710 USA (e-mail: smg84@cam.ac.uk).

Color versions of one or more figures in this article are available at https://doi.org/10.1109/JESTPE.2023.3281760.

Digital Object Identifier 10.1109/JESTPE.2023.3281760

is proposed for both fault-tolerant and active power controls, respectively, through a similar HESS. On the other hand, multilevel converters have been also used to mitigate the variable energy production of renewables in hybrid microgrids, where UCs and batteries are distributed in different branches of an MMC realizing fully decoupled power control and also optimizing the performance of the storage units [21].

Nevertheless, multioutput multilevel (MOM) converters are also an interesting alternative for hybrid systems, either for different loads [22] or for different types of sources [23]. In particular, Cascaded MOM (CMOM) converter has been proposed for hybrid sources systems, since it is composed of m converters that can generate n voltage output terminals [23]. Each of these n voltage outputs can operate with $2m+1$ voltage levels and different amplitude, frequency, and phase angle when the system is within the stable operation region. To allow a modular structure in the dc-bus of the CMOM, with the purpose of incorporating e energy storage units with their own different dynamics, a modular series/parallel interconnection is integrated. This extra degree of freedom in the switching states allows not only the series interconnection among the cells of the converter, i.e., among the energy storage units, but also enables the parallel interconnection of them. In this way, the proposed dc-bus structure for the CMOM enables several benefits: the internal voltage balance among the cells, without extra sensors or control algorithms; and the reduction of the total parasitic inductance and resistance in the energy paths [24], [25], [26], [27], [28].

In this article, a HESS based on a CMOM converter is presented. As the main concept, it combines batteries and capacitors in each module of the converter, in order to implement a hybrid system that features both high-energy and high-power densities. For this proposal, the system is developed for $m = 2$ converters with $n = 2$ output voltage terminals [29], [30]. On the other hand, the internal balance of the storage units is achieved through the series/parallel connection strategy between the energy storage elements. Moreover, the operational region of the proposed converter is analyzed and algebraically demonstrated to limit the references only to the stable operation zone. As long as the system is operating in the region defined as stable, the proposed system can maintain a decoupled control of each ac output without stability or distortion problems.

In this way, it can be resumed that the major contributions of the article.

1) The validation of a novel HESS based on a MOM converter.
2) The use of a series/parallel connection strategy for achieve the internal balance of the heterogeneous storage units, without the need to use extra control loops or sensors to achieve the internal voltage balance between these units.
3) The characterization of the operational region of the proposed system.

II. Proposed MOM Converter Topology

The proposed MOM converter topology (with $m = 2$ converters with $n = 2$ output voltage terminals) is presented in Fig. 1. This novel approach is based on a HESS with a reduced number of battery units. Indeed, the proposed topology offers five voltage levels in each output port with a single battery. The other storage element implemented in the topology is a capacitor, which through the modulation strategy is connected in series and parallel to the battery, leading to balanced voltages between them and increasing the number of levels in each ac output port.

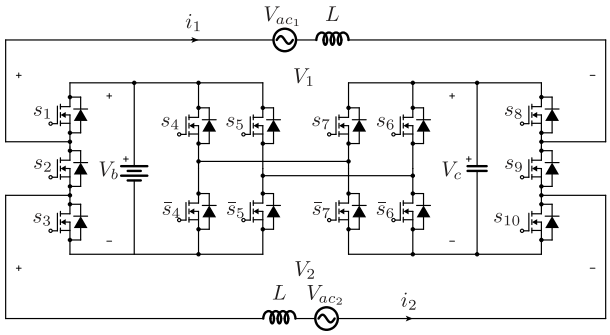

Fig. 1. Proposed dual-output multilevel converter.

TABLE I
CMOM Converters Comparison

Topology	Extension in number of input/output	Multilevel Output capability	Hybrid storage units
V. Jayan et al. [23]	✓	✓	×
V. Jayan et al. [29]	✓	✓	×
Z. Zheng [31]	×	✓	✓
G. Sharon [32]	×	✓	✓
Proposed topology	✓	✓	✓

Several multilevel ESS can be found in the literature, with an important focus in EV applications and grid connection systems. A comparison is presented in Table I, covering several power converters such as the traditional CMOM [23], a cascaded dual-output multilevel converter [29], a hybrid cascaded multilevel converter [31] and finally a Modular Multilevel Converter for Energy Management [32]. All these topologies are evaluated in three main dimensions: 1) the capability of a straightforward extension in the number of input-output terminals; 2) the feature of generating multilevel output voltage waveforms; and 3) the capability of the system to integrate hybrid storage units and allow the internal balance of them. It can be seen that MOM converters allow important benefits compared with traditional 2L-VSC-based solutions, due to the superior quality in the generated voltage waveforms, the capability of redundant states, and the flexibility for increasing the number of input/outputs. From the MOM topologies presented in Table I, the ones from [23] and [29], feature flexibility for achieving multiple input/outputs while maintaining a decoupled control, with the addition of a multilevel output voltage. However, the flexibility to use hybrid storage elements and keep them balanced in a simple way is not feasible. In [31] and [32], different structures and modules are presented. These allow to incorporate hybrid storage elements with a simple control strategy that keeps them balanced. However, the extension for multiple input-output and the capability of decoupled control is not straightforward.

TABLE II
SWITCHING STATES AND OUTPUT VOLTAGES

s_1	s_2	s_3	s_4	s_5	s_6	s_7	s_8	s_9	s_{10}	V_1	V_2
1	0	1	0	1	1	0	1	0	1	0	0
1	1	0	0	1	1	0	1	0	1	0	v_{dc}
1	0	1	0	1	1	0	1	1	0	0	-v_{dc}
1	0	1	0	1	1	0	0	1	1	v_{dc}	0
1	1	0	0	1	1	0	0	1	1	v_{dc}	v_{dc}
1	1	0	0	0	1	1	1	0	1	v_{dc}	$2v_{dc}$
1	0	1	0	0	1	1	0	1	1	$2v_{dc}$	v_{dc}
1	1	0	0	0	1	1	0	1	1	$2v_{dc}$	$2v_{dc}$
0	1	1	0	1	1	0	1	0	1	-v_{dc}	0
0	1	1	1	0	0	1	1	1	0	-v_{dc}	-v_{dc}
1	0	1	1	1	0	0	1	1	0	-v_{dc}	-$2v_{dc}$
0	1	1	1	1	0	0	1	0	1	-$2v_{dc}$	-v_{dc}
0	1	1	1	1	0	0	1	1	0	-$2v_{dc}$	-$2v_{dc}$

The proposed topology comprises 14 semiconductors, besides the storage units and filtering elements. This circuit can generate two ac outputs identified as V_1 and V_2 respectively. Each output waveform features up to five voltage levels, leading to a reduction of the THD of the grid side and therefore, lower filter requirements for connecting to the electrical grid. Thereby, the converter is connected to two different ac systems, each characterized by a reactor (L) and a resistor (R) to model the input filter. Besides, a single-phase ac supply (V_{acx}) where $x = \{1, 2\}$ represents whether is referred to the ac system 1 or 2. For simplicity, in this work, it is assumed that L and R are equal for both systems, but it is important to highlight that this condition is not mandatory.

Then, to achieve the internal voltage balance between the battery unit and the capacitor, the control strategy prioritizes the switching states that connect them in parallel, leading to a simpler balancing without using complex control strategies nor multiple sensors for monitoring the status of these units. For the validation of this parallel operation mode, an interface with parallel-connection capability based on two H-Bridge converters (semiconductors s_4–s_7 and their respective negates) is employed. This decision is to replicate the validation of parallel connection for this topology presented in [25], [33], and [34].

Moreover, it is important to consider the design aspects of the parallel connection presented in the proposed paper. For this consideration, in [26] the evaluation of the effects of different values of capacitance, stray inductances, and the effect of the module switching frequency is discussed. Furthermore, an analysis of the parasitic inductance parameters and losses associated with different semiconductor modules is included, indicating that taking into consideration the typical parasitic values of the semiconductor modules, the current values reached when using the parallel connection between the battery with the capacitor, are within the acceptable range and will not result in current spikes. This feature will be exploited and demonstrated in the remainder of the article. The available switching states and the resulting output voltages are summarized in Table II. It is important to highlight that Table II is conceived assuming that the internal voltage balance between the capacitor and the battery is operating correctly. This leads to the following assumption for Fig. 1: $V_b = V_c = v_{\mathrm{dc}}$

III. MODEL-PREDICTIVE CONTROL STRATEGY

According to the set of feasible states enabled by the converter depicted in Table II, the system is able to generate 13 different voltage conditions. Each of the outputs can be defined as follows:

$$V_1 = (s_1 - s_4)V_b + (s_7 - s_8)V_c \tag{1}$$

$$V_2 = (s_1 s_2 - s_4)V_b + (s_7 - s_8 s_9)V_c \tag{2}$$

where V_b and V_c are the battery and capacitor voltages respectively. From the previous equations, the coupling between the voltage outputs is evident. This will restrict the operation of the ac systems as it will be shown in Section III-B.

Once the converter model has been obtained, it is possible to model the grid interaction. Applying the Kirchhoff's voltage law in both ac systems leads to

$$V_1 = L\frac{\mathrm{d}i_1}{\mathrm{d}t} + Ri_1 + V_{\mathrm{ac_1}} \tag{3}$$

$$V_2 = L\frac{\mathrm{d}i_2}{\mathrm{d}t} + Ri_2 + V_{\mathrm{ac_2}}. \tag{4}$$

A. Prediction Model

With the system properly modeled in the continuous time domain, a prediction model needs to be derived for the control variables, which in this case are the ac input currents i_1 and i_2. Since the control platform and the control scheme are discrete by nature, a discrete model is needed. Hence, by calculating the zero-order hold equivalent, considering a sampling time of h, leads to the following prediction equations for the controlled variables:

$$i_1^p[k+1] = e^{-\frac{h}{\tau_i}} i_1[k] + \frac{1 - e^{-\frac{h}{\tau_i}}}{R_i}\left(V_1[k] - V_{\mathrm{ac_1}}[k]\right) \tag{5}$$

$$i_2^p[k+1] = e^{-\frac{h}{\tau_i}} i_2[k] + \frac{1 - e^{-\frac{h}{\tau_i}}}{R_i}\left(V_2[k] - V_{\mathrm{ac_2}}[k]\right) \tag{6}$$

where $\tau_i = L/R$ is the input filter time constant, $k = nh$ represents the actual sampling instant and $n \in \mathbb{Z}^+$ and h is the sampling period for the FS-MPC algorithm.

Equations (5) and (6) allow predicting the behavior of the control variables for each one of the possible voltages synthesized by the converter. With these quantities available the cost function g can be evaluated by

$$g = \left(i_1^* - i_1^p[k+1]\right)^2 + \left(i_2^* - i_2^p[k+1]\right)^2 \tag{7}$$

where i_1^* and i_2^* are the current references for ac system 1 and 2, respectively. The proposed scheme for the Model predictive control is presented in Fig. 2.

B. Operation Region

Each ac system has a restricted operation region and depends on the maximum modulation index that can achieve. However, in the proposed multioutput converter, there is a coupling factor between the ac outputs, as depicted in (1) and (2), that limits the operation region. In order to characterize the operation region of the proposed system, the steady-state expressions for (3) and (4), are defined by

$$V_1 = i_1^* R + V_{\mathrm{ac_1}} \tag{8}$$

$$V_2 = i_2^* R + V_{\mathrm{ac_2}}. \tag{9}$$

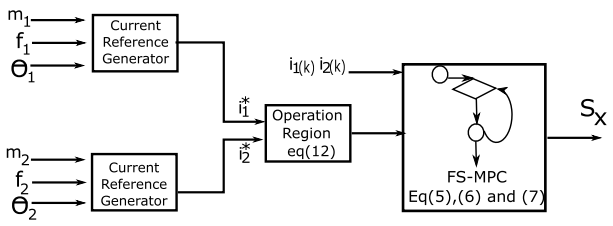

Fig. 2. Model predictive control scheme.

TABLE III
SIMULATION PARAMETERS

Parameter	Symbol	Value
Line Inductance	L	10 mH
Line Resistance	R	0.1 Ω
Battery voltage	v_{dc}	110.4 V
Cell Capacitance	C	1000 μF
Sample Time	h	50 μs

The difference between (8) and (9) is defines the expression $\Delta v_{\rm dc}$

$$\Delta v_{\rm dc} \;=\; V_1 - V_2 = \left(i_1^* R - i_2^* R\right) + \left(V_{\rm ac_1} - V_{\rm ac_2}\right). \qquad (10)$$

Using Table II, it is possible to identify that the maximum $|\Delta v_{\rm dc}|$ is equal to the battery voltage $v_{\rm dc}$, assuming the balance between the capacitor and the battery is correctly implemented. In this way, it is possible to define the maximum deviation expression as

$$|\Delta v_{\rm dc}|_{\rm max} = v_{\rm dc}. \qquad (11)$$

And therefore, applying (11) in (10), it is possible to define the specified region where both systems can operate independently

$$-v_{\rm dc} \le \left(i_1^* R - i_2^* R\right) + \left(V_{\rm ac_1} - V_{\rm ac_2}\right) \;\le\; v_{\rm dc}. \qquad (12)$$

If the current references of ac systems 1 and 2 cause the system to operate outside the region defined in (12), the proposed system will lose the capability to follow both current references in a decoupled manner, besides generating distortion in both currents.

IV. SIMULATION RESULTS

This section evaluates the proposed system with the parameters presented in Table III. To demonstrate the decoupled operation of the system, the operation is analyzed in two different operation modes: in Operation Mode 1 the total system is evaluated under asynchronous operation. Operation Mode 2 the ac system 2 injects power to system 1, with a complementary contribution of the battery unit.

A. Operation Mode 1

For Operation Mode 1, the ac voltage 1 ($V_{\rm ac_1}$) amplitude is 50 V while the ac voltage 2 ($V_{\rm ac_2}$) is 60 V. Moreover, their frequencies are 60 and 50 Hz, respectively, to validate the operation in asynchronous mode. Another important aspect is that the operation of the system is within the stable operation region presented in (12).

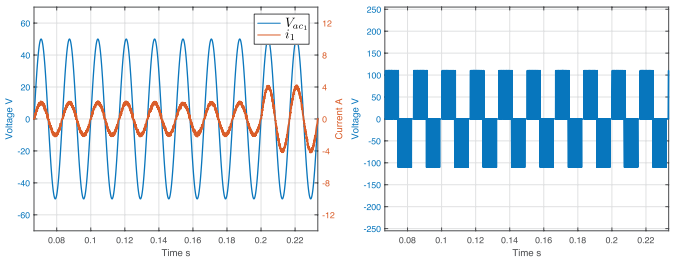

(a) (b)

Fig. 3. Operation Mode 1. (a) AC current and voltage system 1. (b) Converter voltage V_1.

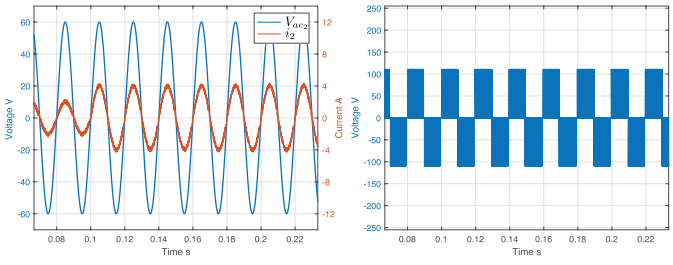

(a) (b)

Fig. 4. Operation Mode 1. (a) AC current and voltage system 2. (b) Converter voltage V_2.

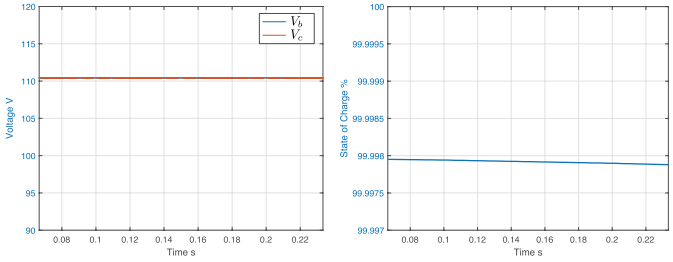

(a) (b)

Fig. 5. Operation Mode 1. (a) Battery voltage V_b and capacitor voltage V_c. (b) Battery SoC.

In Fig. 3(a) the ac voltage and current of system 1 are presented. The figure demonstrates the correct operation of the control strategy, allowing to track a current amplitude step change at $t = 0.2$ s, showing the system being capable of generating this current reference variation and keeping current in phase with the input voltage in terminal 1. The output voltage V_1 generated by the converter is presented in Fig. 3(b), where it is possible to recognize a three-level voltage waveform. On the other hand, Fig. 4(a) presents the ac voltage and current for system 2. In this case, a current step change is implemented at $t = 0.1$ [s] and the system maintains the correct performance over both systems. In Fig. 4(b) the voltage output V_2 is shown. Moreover, the parallel connection between the capacitor and the battery, allows to keep the capacitor voltage balanced and equal to the battery voltage, as presented in Fig. 5(a). Finally, the power flows from the battery to the ac system 1 and 2, resulting in a reduction in the state of charge (SoC) of the battery as shown in Fig. 5(b).

B. Operation Mode 2

As described earlier, during Operation Mode 2 the ac system 2 injects power to system 1, with a complementary contribution from the battery unit. In this scenario, $\hat{V}_{\rm ac_1}$ is

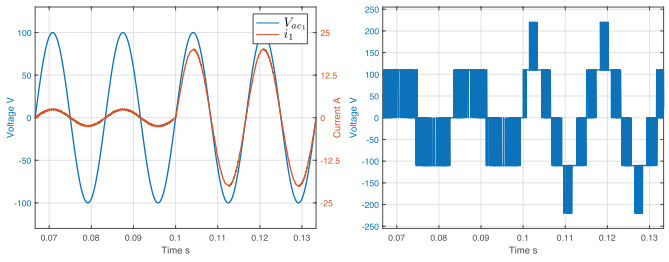

(a) (b)

Fig. 6. Operation Mode 2. (a) AC current and voltage system 1. (b) Converter voltage V_1.

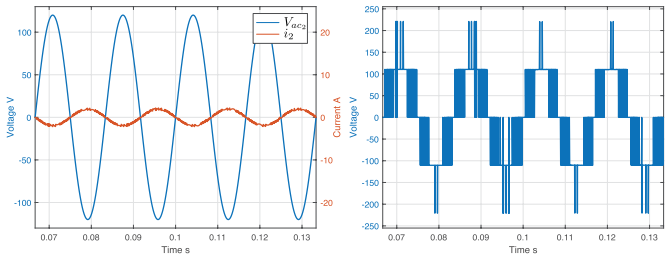

(a) (b)

Fig. 7. Operation Mode 2. (a) AC current and voltage system 2. (b) Converter voltage V_2.

100 V and $\hat{V}_{\text{ac}_2}$ reaches 120 V. The frequency for both ac systems is set to 60 Hz. In Fig. 6(a), the ac system 1 generates an ac current with an amplitude of $\hat{i}_1 = 2.4$. For this operating condition, the current supplied by the ac system 2 has an amplitude of 2 A and appears in counter-phase with its ac supply, like is shown in Fig. 7(a). In this scenario, the power of system 1 is equal to the power of system 2, and therefore, the battery does not charge/discharge and keep constant the SoC, as presented in Fig. 8(b). However, in $t = 0.1$ s the amplitude of the current of the ac system 1 is increased to $\hat{i}_1 = 20$ [A], while the current of the system 2 remains in its previous setpoint ($\hat{i}_2 = 2$ A), as illustrated in Figs. 6(a) and 7(a) respectively. In this case, the difference in power between the ac system 1 and 2 is supplied by the battery unit. For this reason, Fig. 8(b) presents how the SoC of the battery starts to decrease from this instant onward. Then, the results from Fig. 8(a) confirm that the capacitor voltage is kept balanced and equal to the battery voltage throughout the duration of the test. Finally, from Figs. 6(b) and 7(b) it is possible to identify that the ac outputs 1 and 2 are operating with larger modulation indexes than the previous case since they produce five-level voltage waveforms.

C. Efficiency and Power Loss Analysis

Once the operation of the converter has been validated, an evaluation of the system losses will be performed. To further explore the features of the proposed HESSs, the system will be driven and analyzed in different scenarios. To do so, data will be collected for different power consumption from each ac system. The presented results are obtained using the thermal modeling tool in PLECS, while the semiconductor employed for the switches is the SCT4045DR Silicon Carbide from Rohm. Note that the ac systems were sized for their

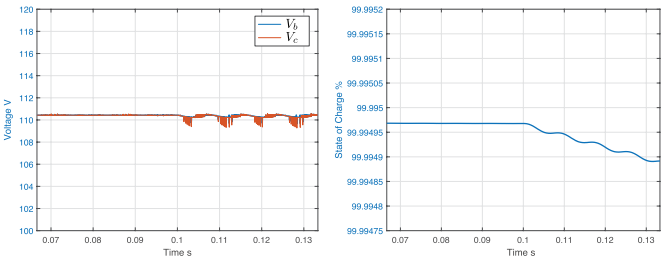

(a) (b)

Fig. 8. Operation Mode 2. (a) Battery voltage V_b and capacitor voltage V_c. (b) Battery SoC.

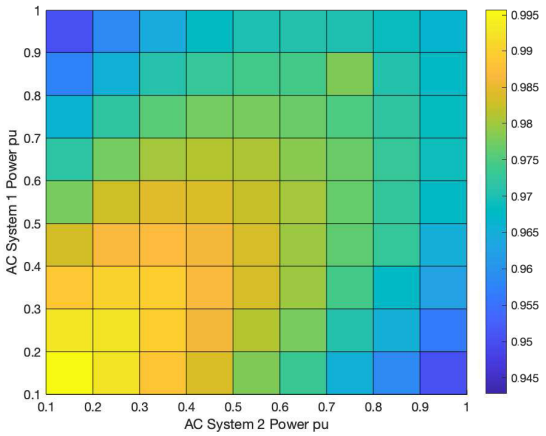

Fig. 9. Simulated efficiency using PLECS.

ratings, in order to provide a realistic measure of the system's losses, while the results in Fig. 9 have been normalized to give a fair comparison. Also, in every scenario, it is assumed that both ac systems are sinking power from the battery, with the switching devices being hard switched.

Fig. 9, displays the overall performance of the HESSs, covering different operating points for each system, the idea was to illustrate how the power consumption in each ac system affects the total conversion efficiency. It can be seen that the multioutput system presents a peak efficiency of 99.57%, while the average efficiency is 97.25%. Fig. 10 depicts the losses distribution of the systems, in order to illustrate which elements concentrate the biggest share of the losses depending on the operation point. Please note that in this case, the system kept one of the ac buses operating at rated power, while the other was varying its consumption. It can be seen that the three-switch (TS) cells concentrate the larger share of losses, almost doubling the losses in the H-bridges at rated power operation, displayed in Fig. 10(a). In this case, the TS cells interfacing the ac side reach 31.5 W of losses, while the HBs totalize about 16 W of losses. Also, given that SiC devices are employed, conduction losses dominate the power loss distribution as presented in Fig. 10(b) and (c).

Interestingly, results also prove that by properly promoting the use of the parallel connection between the cells, the inrush currents can be kept within reasonable amplitude, hence the losses related to it can be reduced as suggested in [26].

V. Experimental Results

The main objective of these experimental results is to demonstrate the versatility of the proposed converter. Thereby,

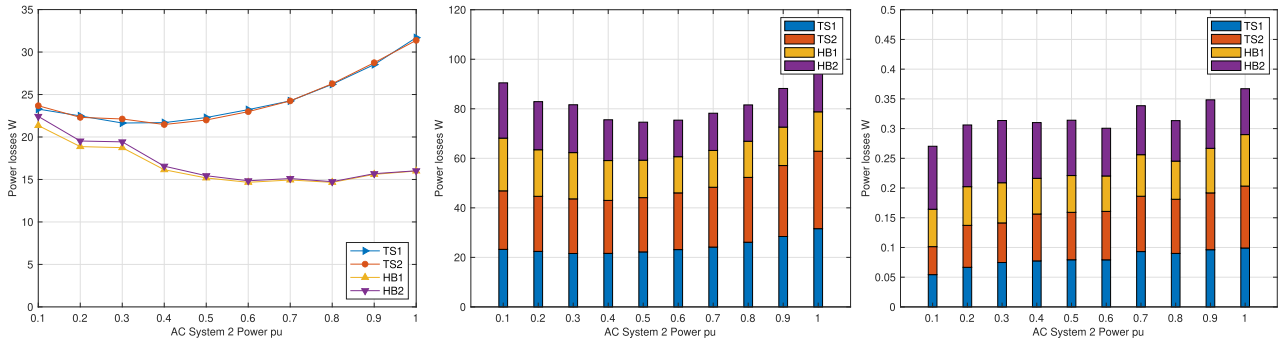

Fig. 10. Power loss distribution per stage. (a) Total losses. (b) Conduction losses. (c) Switching losses.

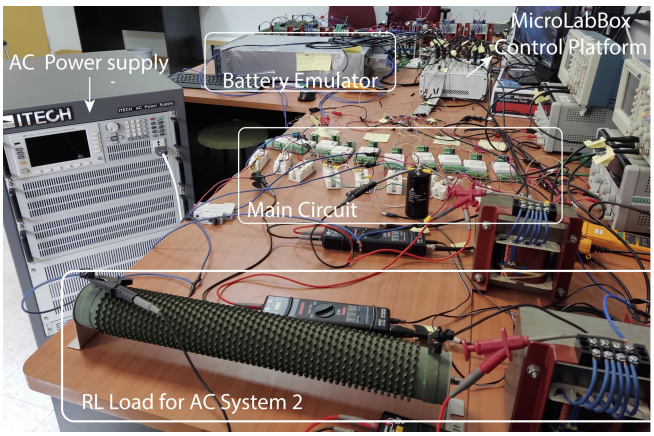

Fig. 11. Dual-output multilevel converter experimental setup.

different scenarios will be evaluated in several operation conditions, besides emphasizing the simplicity to maintain the different storage stages balanced. First, three different operation conditions are evaluated: operation with different current amplitudes, different current phases and with different frequencies for each ac system. These three scenarios are evaluated in both ac systems with an RL load and with the parameters defined in Table IV. These experimental scenarios validate the integration and decoupled control of the ac current of each output, in order to validate the independent control of the active and reactive power, along with the interconnection of two or more asynchronous systems. The developed experimental setup is displayed in Fig. 11.

In addition, results of the system facing a decoupled scenario with different voltage levels at the ac side, besides the validation of the operation of the system as an HESS are included. These additional experimental results demonstrate the capability to generate multilevel voltage waveform outputs, leading to reduced harmonic content in the electrical grid. Moreover, a validation of the system operating as a HESS is included, which confirms the capability to integrate heterogeneous storage systems.

It is important to remark that all the experimental validation is implemented within the stable operation region defined in (12).

A. Operation With Different Current Amplitudes

To validate the operation modes of the system with different amplitudes of the current for both systems. Please note that

TABLE IV
EXPERIMENTAL PARAMETERS

Parameter	Symbol	Value
Line Inductance	L	15 mH
Line Resistance	R	10 Ω
Battery voltage	v_{dc}	50 V
Cell Capacitance	C	1000 μF
Sample Time	h	50 μs

the current references for ac systems are defined with the same phase and frequency (50 Hz). During all the tests, the current reference for the ac system 1 is kept controlled to an amplitude of 2 A, which is validated through Fig. 12(a), as the measured current from this system is following it perfectly. On the other hand, the current reference of the ac system 2 initially is set to 0.5 A, and after a while is changed to 2 A. The measurements for current i_2 show a perfect tracking of it reference, while the other system remains unchanged. These results confirm the decoupled control of each ac output.

In Fig. 12(b), the converter voltages of system 1 and 2 are shown. It is possible to identify clearly the three-level voltage operation. Fig. 12(c) presents the capacitor voltage of the proposed topology, demonstrating that the parallel connection between the battery and the capacitor permits to maintain the voltage balance over the storage elements during all the operation of the system.

B. Operation With Different Current Phases

The operation of the ac system 1 and 2 with different phases of the current references is validated in this section. The current amplitudes are set to 1 A and the frequencies of both ac systems is 50 Hz. The phase difference between ac system 1 and 2 is equivalent to 90°, as shown in Fig. 13(a). Fig. 13(b) and (c) present the converter voltage and the capacitor voltage, respectively. It is clear that the operation is totally stable and validates the decoupled operation of system 1 and 2 under phase shift of the current references of ac systems 1 and 2. Additionally, the energy storage stages remain perfectly balanced throughout the test.

C. Operation With Different Current Amplitude and Frequency

Fig. 14(a) exhibits the ac currents and their references. In this scenario, the current reference of the ac system 1 has an

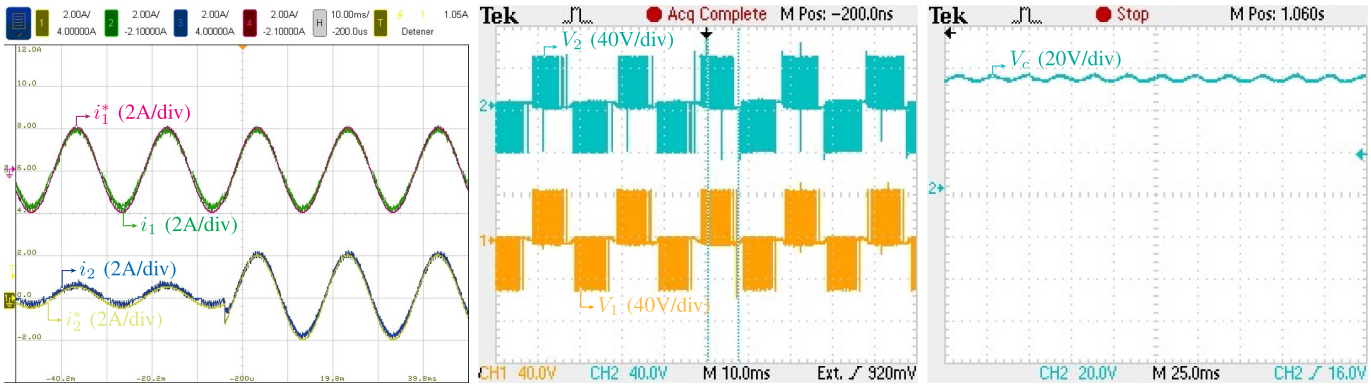

(a) (b) (c)

Fig. 12. Operation with different current amplitudes. (a) CH1: current reference ac system 2, 2 A/div; CH2: measured current ac system 1, 2 A/div; CH3: measured current ac system 2, 2 A/div; CH4: current reference ac system 1, 2 A/div. (b) CH1: converter voltage ac system 1, 40 V/div; CH2: Converter voltage ac system 2, 40 V/div. (c) Capacitor voltage, 20 V/div.

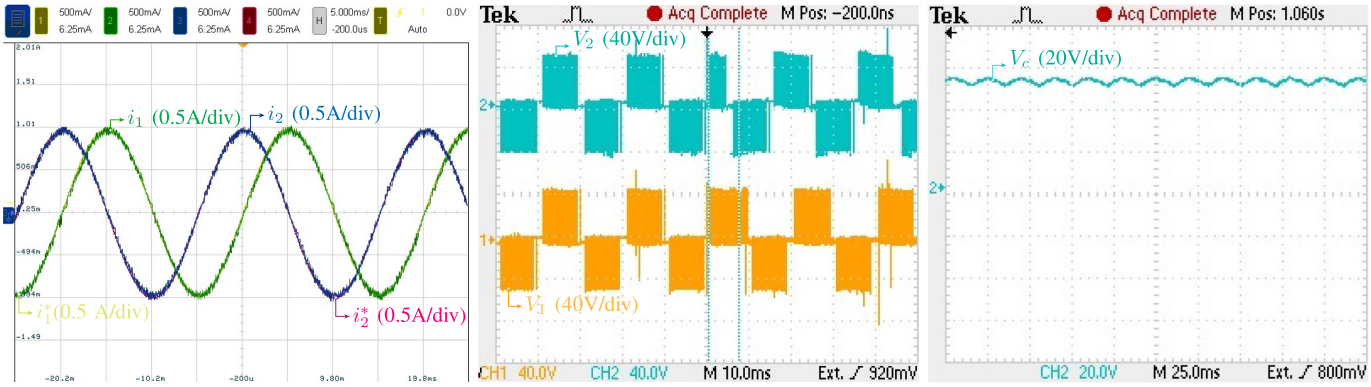

(a) (b) (c)

Fig. 13. Operation with different current phases. (a) CH1: current reference ac system 1, 0.5 A/div; CH2: measured current ac system 1, 0.5 A/div; CH3: measured current ac system 2, 0.5 A/div; CH4: current reference ac system 2, 0.5 A/div. (b) CH1: Converter voltage ac system 1, 40 V/div; CH2: Converter voltage ac system 2, 40 V/div. (c) Capacitor voltage, 20 V/div.

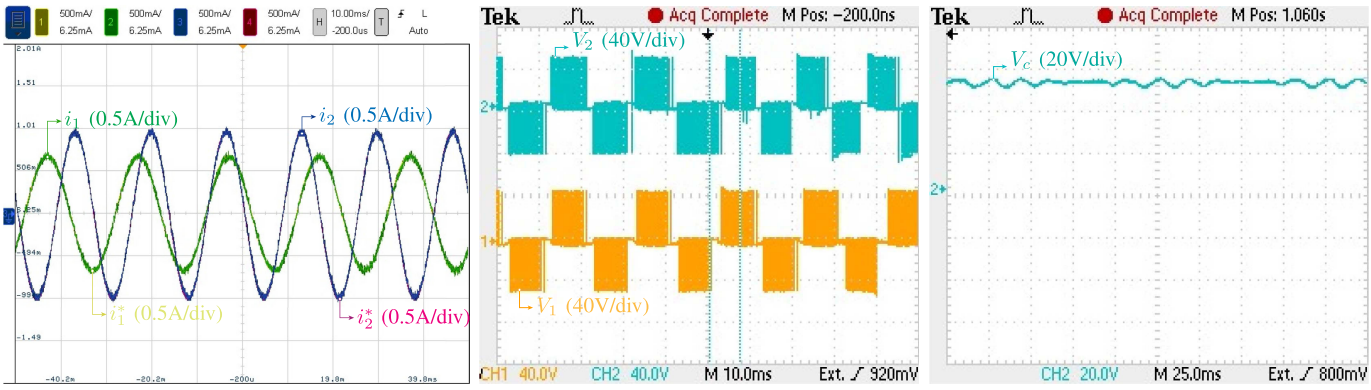

(a) (b) (c)

Fig. 14. Operation with different current amplitude and frequency. (a) CH1: current reference ac system 1, 0.5 A/div; CH2: measured current ac system 1, 0.5 A/div; CH3: measured current ac system 2, 0.5 A/div; CH4: current reference ac system 2, 0.5 A/div. (b) CH1: converter voltage ac system 1, 40 V/div; CH2: converter voltage ac system 2, 40 V/div. (c) Capacitor voltage, 20 V/div.

amplitude equivalent to 0.7 A and 50 Hz, while ac system 2 is set to track a signal with an amplitude of 1 A and 60 Hz. The proposed multioutput converter allows the decoupled control without distortion due to the restriction of operation under a stable operation region. In Fig. 14(b) the converter voltages are correctly synthesized. Finally, Fig. 14(c) shows the evolution of the capacitor voltage, which is also balanced with the battery voltage. This balance permits to maintain the multilevel voltage waveforms and therefore a high-power quality.

D. Operation With Maximum Voltage Levels

To demonstrate the capability of the proposed converter to generate five-level waveforms in both ac voltage outputs, the following test is illustrated in Fig. 15. In this case, the first

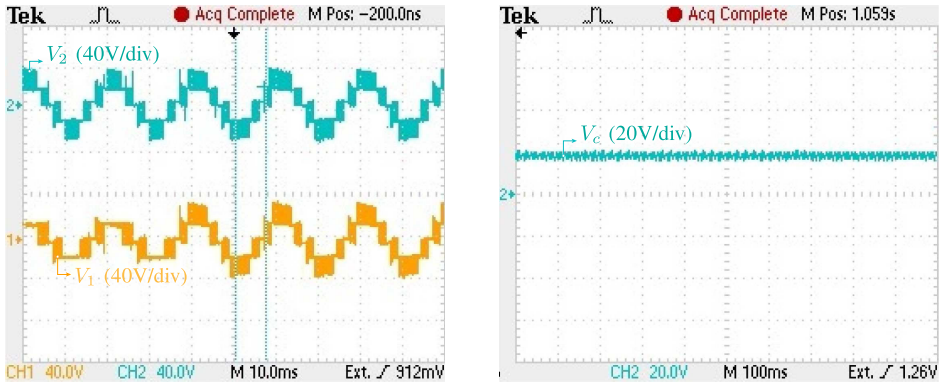

(a) (b)

Fig. 15. Operation with maximum voltage levels. (a) CH1: converter voltage ac system 1, 40 V/div; CH2: converter voltage ac system 2, 40 V/div. (b) Capacitor voltage; 20 V/div.

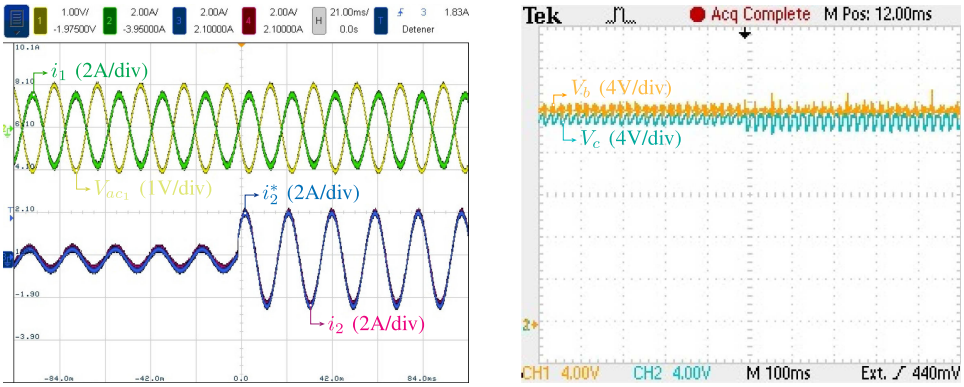

(a) (b)

Fig. 16. HESS Operation. (a) CH1: Normalized ac voltage of system 1, 1 V/div; CH2: measured current ac system 1, 2 A/div; CH3: current reference ac system 2, 2 A/div; CH4: measured current ac system 2, 2 A/div. (b) CH1: Battery voltage, 4 V/div; CH2: capacitor voltage, 4 V/div.

stage, the voltage of the ac system 1 has three voltage levels meanwhile the output voltage of the system 2 has five levels as displayed in Fig. 15(a). Then, a step change in the reference is performed in the modulation indexes in order to get in both the systems voltage waveforms with five defined levels. In Fig. 15(b) it is possible to appreciate the capacitor voltage balanced during all the tests. It is important to highlight the fact that the capacitor voltage balance is the key to achieving a proper multilevel waveform.

E. HESS Operation

Finally, the capability of the system to operate as HESS is shown in Fig. 16. Fig. 16(a) shows how a load impact from 0.5 to 2 A is applied to in the ac system 2. In the ac system 1, a grid voltage is connected as a load. The ac system 1 current and grid voltage are presented in Fig. 16(a), noting that they remain constant, regardless of the impact on the load of the ac system 2. When generating a power difference between ac system 1 and 2, the power difference is delivered by the storage system incorporated in the proposed system. In Fig. 16(b) it is observed how the dynamic response of the capacitor acts faster than the dynamics of the battery, which is one of the interesting characteristics of HESS systems, allowing the implementation of storage systems with high energy and power density.

VI. Conclusion

This article presents a HESS based on a Cascade MOM converter. The proposed topology features the usage of different storage units, being able to keep them balanced due to the capability of achieving dynamic interconnection of them in either series or parallel. Hence, the system is capable to allow a sensorless energy and voltage balancing strategy. Also, the system is able to connect the HESS simultaneously to different ac systems, besides the capability of actively increasing the number of voltage levels generated at the output ports.

Moreover, the proposal demonstrates the stable region where the CMOM converter can interact with different ac systems in a decoupled control manner, achieving a stable and high-performance operation. For the validation of the performance of the proposed HESS based on a MOM converter and control strategy, the system was evaluated under different operation conditions for the ac outputs, such as grids with different amplitudes, frequencies, or phase shifts. Along with these results, the validation of the proposed system as an HESS given energy support to the integrated system is validated with experimental results.

Finally, in all the experimental results, the controller achieves a stable and high-performance operation, which demonstrates the feasibility of implementation of hybrid storage system using CMOM topologies. These results present the proposed solution as a valid option for the integration of microgrids based on different energy sources and storage units, interconnecting asynchronous ac systems, and enabling flexible energy paths.

REFERENCES

[1] C. J. Joubert, N. Chokani, and R. S. Abhari, "Impact of large scale battery energy storage on the 2030 central European transmission grid," in *Proc. 15th Int. Conf. Eur. Energy Market (EEM)*, Jun. 2018, pp. 1–5.

[2] M. Stecca, L. R. Elizondo, T. B. Soeiro, P. Bauer, and P. Palensky, "A comprehensive review of the integration of battery energy storage systems into distribution networks," *IEEE Open J. Ind. Electron. Soc.*, vol. 1, pp. 46–65, 2020.

[3] S. Stynski, W. Luo, A. Chub, L. G. Franquelo, M. Malinowski, and D. Vinnikov, "Utility-scale energy storage systems: Converters and control," *IEEE Ind. Electron. Mag.*, vol. 14, no. 4, pp. 32–52, Dec. 2020.

[4] N. Kawakami and Y. Iijima, "Overview of battery energy storage systems for stabilization of renewable energy in Japan," in *Proc. Int. Conf. Renew. Energy Res. Appl. (ICRERA)*, Nov. 2012, pp. 1–5.

[5] W. Luo, S. Stynski, A. Chub, L. G. Franquelo, M. Malinowski, and D. Vinnikov, "Utility-scale energy storage systems: A comprehensive review of their applications, challenges, and future directions," *IEEE Ind. Electron. Mag.*, vol. 15, no. 4, pp. 17–27, Dec. 2021.

[6] L. Argiolas, M. Stecca, L. M. Ramirez-Elizondo, T. B. Soeiro, and P. Bauer, "Optimal battery energy storage dispatch in energy and frequency regulation markets while peak shaving an EV fast charging station," *IEEE Open Access J. Power Energy*, vol. 9, pp. 374–385, 2022.

[7] L. Wang, Z. Qin, T. Slangen, P. Bauer, and T. van Wijk, "Grid impact of electric vehicle fast charging stations: Trends, standards, issues and mitigation measures—An overview," *IEEE Open J. Power Electron.*, vol. 2, pp. 56–74, 2021.

[8] G. G. Farivar et al., "Grid-connected energy storage systems: State-of-the-art and emerging technologies," *Proc. IEEE*, vol. 111, no. 4, pp. 397–420, Apr. 2023.

[9] S. Rivera et al., "Charging infrastructure and grid integration for electromobility," *Proc. IEEE*, vol. 111, no. 4, pp. 371–396, Apr. 2023.

[10] D. Parra, S. A. Norman, G. S. Walker, and M. Gillott, "Optimum community energy storage for renewable energy and demand load management," *Appl. Energy*, vol. 200, pp. 358–369, Aug. 2017.

[11] R. Hemmati and H. Saboori, "Short-term bulk energy storage system scheduling for load leveling in unit commitment: Modeling, optimization, and sensitivity analysis," *J. Adv. Res.*, vol. 7, no. 3, pp. 360–372, May 2016.

[12] B. P. Roberts and C. Sandberg, "The role of energy storage in development of smart grids," *Proc. IEEE*, vol. 99, no. 6, pp. 1139–1144, Jun. 2011.

[13] J. Shen and A. Khaligh, "A supervisory energy management control strategy in a battery/ultracapacitor hybrid energy storage system," *IEEE Trans. Transport. Electrific.*, vol. 1, no. 3, pp. 223–231, Oct. 2015.

[14] S. M. Lukic, S. G. Wirasingha, F. Rodriguez, J. Cao, and A. Emadi, "Power management of an ultracapacitor/battery hybrid energy storage system in an HEV," in *Proc. IEEE Vehicle Power Propuls. Conf.*, Sep. 2006, pp. 1–6.

[15] H. Abu-Rub, J. Holtz, J. Rodriguez, and G. Baoming, "Medium-voltage multilevel converters—State of the art, challenges, and requirements in industrial applications," *IEEE Trans. Ind. Electron.*, vol. 57, no. 8, pp. 2581–2596, Aug. 2010.

[16] A. Dekka, B. Wu, and N. R. Zargari, "A novel modulation scheme and voltage balancing algorithm for modular multilevel converter," *IEEE Trans. Ind. Appl.*, vol. 52, no. 1, pp. 432–443, Jan. 2016.

[17] S. Rivera, Z. Li, J. Luo, A. V. Peterchev, and S. M. Goetz, "Modular multilevel series/parallel converter with switched-inductor energy transfer between modules," *IEEE Trans. Power Electron.*, vol. 34, no. 5, pp. 4844–4852, May 2019.

[18] M. Correa and S. Rivera, "Hybrid energy storage system based on modular multilevel series parallel converter," in *Proc. 48th Annu. Conf. IEEE Ind. Electron. Soc.*, Oct. 2022, pp. 1–5.

[19] W. Jiang, C. Zhu, S. Xue, K. Ren, and C. Yang, "DC-side-fault-tolerant control of a battery-supercapacitor hybrid energy storage system based on cascaded multilevel converter and auxiliary power loop," *IEEE Trans. Ind. Electron.*, vol. 67, no. 9, pp. 7451–7460, Sep. 2020.

[20] W. Jiang, C. Zhu, C. Yang, L. Zhang, S. Xue, and W. Chen, "The active power control of cascaded multilevel converter based hybrid energy storage system," *IEEE Trans. Power Electron.*, vol. 34, no. 8, pp. 8241–8253, Aug. 2019.

[21] L. Zhang, Y. Tang, S. Yang, and F. Gao, "Decoupled power control for a modular-multilevel-converter-based hybrid AC–DC grid integrated with hybrid energy storage," *IEEE Trans. Ind. Electron.*, vol. 66, no. 4, pp. 2926–2934, Apr. 2019.

[22] P. C. D. Goud and R. Gupta, "Modular multi-output hybrid converter for residential hybrid loads," *IEEE J. Emerg. Sel. Topics Power Electron.*, vol. 10, no. 4, pp. 3840–3850, Aug. 2022.

[23] V. Jayan, A. S. Hussein, and A. Ghias, "Model predictive control of cascaded multi-output multilevel converter," in *Proc. IEEE Int. Conf. Ind. Technol. (ICIT)*, Feb. 2019, pp. 1247–1251.

[24] S. M. Goetz, Z. Li, X. Liang, C. Zhang, S. M. Lukic, and A. V. Peterchev, "Control of modular multilevel converter with parallel connectivityapplication to battery systems," *IEEE Trans. Power Electron.*, vol. 32, no. 11, pp. 8381–8392, Mar. 2017.

[25] Z. Li, R. Lizana F., S. Sha, Z. Yu, A. V. Peterchev, and S. M. Goetz, "Module implementation and modulation strategy for sensorless balancing in modular multilevel converters," *IEEE Trans. Power Electron.*, vol. 34, no. 9, pp. 8405–8416, Sep. 2019.

[26] R. Lizana F. et al., "Modular multilevel series/parallel converter for bipolar DC distribution and transmission," *IEEE J. Emerg. Sel. Topics Power Electron.*, vol. 9, no. 2, pp. 1765–1779, Apr. 2021.

[27] Z. Li, R. Lizana, S. M. Lukic, A. V. Peterchev, and S. M. Goetz, "Current injection methods for ripple-current suppression in delta-configured split-battery energy storage," *IEEE Trans. Power Electron.*, vol. 34, no. 8, pp. 7411–7421, Aug. 2019.

[28] Z. Li, R. Lizana, A. V. Peterchev, and S. M. Goetz, "Distributed balancing control for modular multilevel series/parallel converter with capability of sensorless operation," in *Proc. IEEE Energy Convers. Congr. Expo. (ECCE)*, Oct. 2017, pp. 1787–1793.

[29] V. Jayan and A. M. Y. M. Ghias, "Operational limits of a cascaded dual-output multilevel converter using model predictive control," *IEEE Trans. Power Electron.*, vol. 36, no. 6, pp. 7026–7037, Jun. 2021.

[30] V. Jayan and A. Ghias, "Cascaded dual output multilevel converter to enhance power delivery and quality," in *Proc. IEEE Energy Convers. Congr. Expo. (ECCE)*, Sep. 2019, pp. 2910–2915.

[31] Z. Zheng, K. Wang, L. Peng, Y. Li, and L. Xu, "A hybrid cascaded multi-level converter for power storage system," in *Proc. 15th Eur. Conf. Power Electron. Appl. (EPE)*, Sep. 2013, pp. 1–10.

[32] S. S. George and M. O. Badawy, "A modular multi-level converter for energy management of hybrid storage system in electric vehicles," in *Proc. IEEE Transp. Electrific. Conf. Expo (ITEC)*, Jun. 2018, pp. 336–341.

[33] Z. Li, R. Lizana, Z. Yu, S. Sha, A. V. Peterchev, and S. M. Goetz, "Modulation and control of series/parallel module for ripple-current reduction in star-configured split-battery applications," *IEEE Trans. Power Electron.*, vol. 35, no. 12, pp. 12977–12987, Dec. 2020.

[34] Z. Li, R. Lizana F., Z. Yu, S. Sha, A. V. Peterchev, and S. M. Goetz, "A modular multilevel series/parallel converter for a wide frequency range operation," *IEEE Trans. Power Electron.*, vol. 34, no. 10, pp. 9854–9865, Oct. 2019.

Ricardo Lizana (Senior Member, IEEE) was born in Rancagua, Chile, in 1985. He received the M.Sc. and D.Sc. degrees in electronic engineering from Universidad Tecnica Federico Santa Maria, Valparaíso, Chile, in 2011 and 2015, respectively.

He joined the Universidad Católica de la Santísima Concepción, Concepción, Chile, in 2015, where he is currently an Assistant Professor with the Departamento de Ingenieróa Elêctrica, Santiago, Chile. In 2017, he was a Post-Doctoral Fellow with Duke University Durham, NC, USA. His main research interests include high power converters, HVdc transmission systems, and renewable energy systems.

Dr. Lizana received the Ph.D. Scholarship from the Chilean National Commission for Scientific and Technological Research (CONICYT) in 2011, the Emerging Leaders in the Americas Program Scholarship from the Canadian Bureau for International Education in 2012, the Second Prize Paper Award of IEEE TRANSACTIONS ON POWER ELECTRONICS in 2015, and *IEEE Industrial Electronics Magazine* Best Paper Award in 2022.

Sebastian Rivera (Senior Member, IEEE) received the M.Sc. degree in electronics engineering from Universidad Tecnica Federico Santa Maria (UTFSM), Valparaíso, Chile, in 2011, and the Ph.D. degree (Hons.) in electrical and computer engineering from Ryerson University, Toronto, ON, Canada, in 2015.

From 2016 to 2017, he was a Post-Doctoral Fellow with the University of Toronto, Toronto, and the Advanced Center of Electrical and Electronic Engineering (AC3E), UTFSM. From 2018 to 2022, he was with the Faculty of Engineering and Applied Sciences, Universidad de los Andes, Santiago, Chile. Since 2023, he has been working as a Faculty Member of the Department of Electrical Sustainable Energy, Delft University of Technology, Delft, The Netherlands, and part of the dc Systems, Energy Conversion and Storage Group. He is also an Associate Investigator with the AC3E and the Solar Energy Research Center (SERC-Chile), both centers of excellence in Chile. His research focuses on dc distribution systems, electric-vehicle charging infrastructure, high efficiency dc–dc conversion, multilevel converters, and renewable energy conversion systems.

Dr. Rivera was a recipient of the 2022 *IEEE Industrial Electronics Magazine* Best Paper Award, the Academic Gold Medal of the Governor General of Canada in 2016, the Ph.D. Scholarship from the Chilean National Commission for Scientific and Technological Research (CONICYT) in 2011, and the Emerging Leaders in the Americas Program Scholarship from Canada Global Affairs and the Canadian Bureau for International Education in 2010.

Fidel Figueroa (Student Member, IEEE) was born in Talcahuano, Chile. He received the Electrical Engineering degree from the Universidad Católica de la Santèsima Concepción, Concepción, Chile, in 2021.

He is currently working as a Regulatory Engineer with Coelcha, Cabrero, Chile. His research interests include energy storage systems, multilevel converters, and renewable energy applications.

Freddy Flores-Bahamonde (Senior Member, IEEE) was born in Osorno, Chile, in 1983. He received the M.Sc. and Ph.D. degrees in electronics engineering from Universitat Rovira i Virgili (URV), Tarragona, Spain, in 2009 and 2013, respectively.

In 2015, he joined to the Advanced Center for Electrical and Electronic Engineering (AC3E), Universidad Técnica Federico Santa Maréa (UTFSM), Valparaíso, Chile, as a Post-Doctoral Fellow. In 2017, he was in charge of the energy area in the Technology Transfer Unit of the AC3E developing and managing industrial projects related to the energy and electric power systems field. He is currently an Assistant Professor with the Engineering Sciences Department, Universidad Andres Bello, Santiago, Chile, where he is also the Director of the Energy Transformation Center. His main interests include the design and control of power converters for renewable energies, automotive power systems, and dc microgrids.

Jose Rodriguez (Life Fellow, IEEE) received the Engineer degree in electrical engineering from Universidad Técnica Federico Santa Marèa, Valparaíso, Chile, in 1977, and the Dr.Ing. degree in electrical engineering from the University of Erlangen, Erlangen, Germany, in 1985.

He has been with the Department of Electronics Engineering, Universidad Técnica Federico Santa María, since 1977, where he was a Full Professor and the President. From 2015 to 2019, he was the President with the Universidad Andrés Bello, Santiago, Chile. Since 2022, he has been the President with the Universidad San Sebastian, Santiago. He has coauthored two books, several book chapters, and more than 700 journal articles and conference papers. His main research interests include multilevel inverters, new converter topologies, control of power converters, and adjustable-speed drives.

Dr. Rodriguez is a member of the Chilean Academy of Engineering. He received a number of best paper awards from the IEEE journals. In 2014, he received the National Award of Applied Sciences and Technology from the Government of Chile. In 2015, he received the Eugene Mittelmann Award from the IEEE Industrial Electronics Society. From 2014 to 2022, he was included in the list of Highly Cited Researchers published by Web of Science.

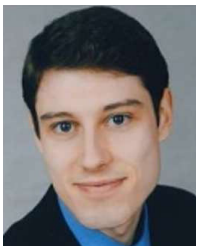

Stefan M. Goetz (Member, IEEE) received the Undergraduate and Graduate degrees from the Technical University of Munich (TU Muenchen), Munich, Germany, in 2007 and 2008, respectively, and the Ph.D. degree from TU Muenchen and Columbia University, New York, NY, USA, in 2012, with a thesis on medical applications of power electronics.

He is currently a Faculty Member of Duke University, Durham, NC, USA, and the University of Cambridge, Cambridge, U.K. He has previously worked in the automotive industry in various positions and levels with a focus on electric drive trains, machines, power electronics, and vehicle architecture. He furthermore developed automotive chargers and charging technologies, which are installed on vehicles and in charging stations around the world. He has worked on grid integration and grid-stabilizing functions of chargers. His research interests include high-quality, high-power, high-bandwidth electronics and magnetics for drive and medical applications, and integrative power electronics solutions for microgrids and electric vehicles.

Dr. Goetz was a recipient of the 2022 *IEEE Industrial Electronics Magazine* Best Paper Award. He was awarded the Ph.D. Thesis Prize from TU Muenchen.